Methods for addressing the protein-protein interaction between histone deacetylase 6 and ubiquitin

Carolina dos S. Passos,[1,2,*] Nathalie Deschamps,[1,*] Yun Choi,[2] Robert E. Cohen,[2] Remo Perozzo,[1] Alessandra Nurisso,[1,3,¶] Claudia A. Simões-Pires,[1,¶]

[1] School of Pharmaceuticals Sciences, University of Geneva, Geneva, Switzerland

[2] Department of Biochemistry & Molecular Biology, Colorado State University, Fort Collins, USA

[3] Department of Biochemistry and Molecular Medicine, University of Montreal, Montreal, Quebec, Canada.

*Contributed equally.

[¶] Corresponding authors: claudia.avello@unige.ch; alessandra.nurisso@unige.ch

Addresses:

School of Pharmaceutical Sciences, University of Geneva, CMU - Rue Michel Servet 1, CH-1211 Geneva 4, Switzerland.

Department of Biochemistry & Molecular Biology, Colorado State University, MRB Building, 1870 Campus Delivery, Fort Collins, CO 80523-1870, USA.

Department of Biochemistry and Molecular Medicine, University of Montreal, C.P. 6128, Montreal, Quebec, H3C 3J7, Canada.

Abstract

Histone deacetylase 6 (HDAC6) is a cytoplasmic HDAC isoform able to remove acetyl groups from cellular substrates such as α-tubulin. In addition to the two deacetylase domains, HDAC6 has a C-terminal zinc-finger ubiquitin (Ub)-binding domain (ZnF-UBP) able to recognize free Ub. HDAC6-Ub interaction is key in regulating the elimination of misfolded proteins during stress response through the aggresome pathway. Small molecules inhibiting deacetylation by HDAC6 were shown to reduce aggresomes, but the interplay between HDAC6 catalytic activity and Ub-binding function is not fully understood. Here we describe two methods to measure HDAC6-Ub interaction *in vitro* using full-length HDAC6. Our results suggest a potential role for the HDAC6 deacetylase domains in modulating HDAC6-Ub interaction. Both methods were effective for screening inhibitors of the HDAC6-Ub protein-protein interaction devoid of catalytic activity. This new HDAC6 modulation mechanism can be targeted to address the function of HDAC6-Ub interaction in normal and disease conditions.

Histone deacetylases (HDACs) are histone-modifying enzymes associated with several cell mechanisms, and of note, the transcriptional regulation of tumor repressor genes. They have been extensively considered as a target in drug discovery for cancer therapy leading to the development of small molecules as catalytic HDAC inhibitors.[1] Although transcriptional regulation is one of the mechanisms involved in the efficacy of HDAC inhibitors, part of the mode of action of pan-inhibitors has been associated with the catalytic inhibition of HDAC6, a cytosolic isoform. The role of HDAC6 in the clearance of misfolded proteins is of particular interest. Upon proteasome impairment, ubiquitin (Ub)-conjugated protein aggregates are recruited by HDAC6, as a compensatory pathway of elimination.[2, 3] The combination of proteasome inhibitors with HDAC6 catalytic inhibitors has been proven to be effective in multiple myeloma, encouraging the development of deacetylase inhibitors selective to HDAC6 for clinical applications.[2-4]

HDAC6 is particular in the fact that it possesses two catalytic deacetylase domains (CD1 and CD2) and a C-terminal zinc-finger Ub-binding domain (ZnF-UBP)[5] (**Fig. 1a**). Strong evidence suggests that intact CD1, CD2, and ZnF-UBP domains play a role in regulating aggresome formation and clearance by HDAC6,[6, 7] with speculations on a possible decrease in HDAC6-Ub interaction upon treatment with the selective HDAC6 inhibitor tubastatin A.[8] Nevertheless, the mechanisms on how catalytic inhibitors of HDAC6 might modulate this specific interaction remained unclear until now. One hypothesis is that the catalytic inhibition would ultimately promote HDAC6 cell de-localization, changing the HDAC6 protein-protein interaction (PPI) profile. Another hypothesis is that the binding of small molecules to the catalytic domains of HDAC6 would promote conformational changes resulting in the disruption of the interaction between HDAC6 ZnF-UBP and Ub. The latter can only be assessed by cell-free protein interaction assays using full-length HDAC6. Up to now, a diversity of binding methods using the HDAC6 ZnF-UBP domain alone have been considered to address the modulation of the HDAC6-Ub interaction.[9, 10] However, they are not suitable for investigating the implications of the catalytic deacetylase domains in the HDAC6-Ub interaction. Here we describe two *in vitro* methods allowing 1) to evaluate the interplay between catalytic domains and the ZnF-UBP in HDAC6, and 2) to retrieve small molecules interacting with the ZnF-UBP leading to HDAC6-Ub PPI inhibition.

Results and discussion

First, we adapted a microscale thermophoresis (MST) method, using human full-length HDAC6, to detect the specific binding of proteins and small drug-like molecules to the HDAC6 ZnF-UBP domain. MST is a fluorescence-based technique with a wide range of applications in the study of biomolecular interactions. Binding of molecules to a fluorescent partner will impact its thermophoretic behavior due to changes in the hydration shell, size, and charge upon binding. In addition, the method can be used to evaluate changes in the temperature jump (T-Jump), which are triggered when binding occurs close to the fluorophore environment. Another advantage of MST is the fact that proteins can be expressed in cells directly as fusion fluorescent proteins, avoiding subsequent labeling chemistry or immobilization steps that may be deleterious to protein folding and activity.[11] As a matter of fact, we have previously experienced loss of binding activity of the full-length HDAC6 while attempting amino coupling reactions for labeling (in MST approach) or immobilization on surface plasmon resonance (SPR) supports (data not shown).

To provide suitable fluorescent interaction partners, HEK 293 cells were transiently transfected with full-length HDAC6-EGFP constructs to obtain the wild type (HDAC6-EGFP WT), the catalytic deficient (HDAC6-EGFP CD), and the ZnF-UBP deleted (HDAC6-EGFP ΔZnF-UBP) proteins, separately (**Fig. 1a,b**). In all these constructs, EGFP was fused to HDAC6 C-terminus, which is closely located to ZnF-UBP. Then, MST experiments were conducted with the whole cell lysates to increase HDAC6 folding stability and maintain its catalytic activity at the same time (**Fig. S1**). HDAC6-Ub binding curves using lysates containing HDAC6-EGFP WT, CD, and ΔZnF-UBP proteins were obtained by evaluating thermophoresis + T-Jump (**Fig. 1c**). The dissociation constant (K_D) for the interaction between mono-Ub with the full length HDAC6-EGFP WT was determined (K_D = 1 μM). Experiments with different dilutions of lysates from cells transfected with HDAC6-EGFP WT showed similar K_D values for the HDAC-Ub interaction suggesting no significant interference by endogenous free Ub, Ub-chains, or Ub-like proteins (**Fig. S2**). The K_D for His-tag Ub binding to HDAC6 was in accordance with previously published ITC data using the ZnF-UBP domain

alone[12] (**Fig. S3**). HDAC6 mutations H216A/H611A leading to total catalytic impairment (HDAC6-EGFP CD) resulted in absence of the HDAC6-Ub interaction (**Fig. 1c**), suggesting that structural changes in the catalytic domains directly affect the Ub-binding activity of HDAC6. Binding studies with Ub-chains and Ub-like proteins (**Fig. S4-5**) were also conducted to confirm the versatility of the method and its application in determining affinity constants of PPI *in vitro*.

A second important application of the method is the screening of small molecules able to interact with HDAC6 residues involved in Ub recognition and potentially acting as direct PPI inhibitors. To demonstrate this application, a structure based virtual screening (SBVS) was first conducted to identify potential compounds targeting the HDAC6 ZnF-UBP.[9, 13] From a chemical library of 197,477 compounds (www.specs.net, SC_specs_10 mg_May2013), 40 potential hits (**Table S1**) were selected and tested by MST for their binding to HDAC6-EGFP WT using thermophoresis + T-Jump (**Fig. 2a**). This measurement provided a suitable Z-factor (0.6) for medium throughput screening and included the contribution of the ZnF-UBP binding via T-Jump. Given the absence of small drug-like molecules able to bind HDAC6 ZnF-UBP or other ZnF-UBP domains, we used 50 µM mono-Ub as a positive binding control for the screening experiments. Therefore, aiming to compare and rank the screened molecules, normalized fraction bound values were determined by comparing the MST curves of the tested compounds to those obtained for the unbound (lysate alone) and bound (lysates pre-incubated with 50 µM mono-Ub) controls. A normalized fraction bound of 0.5 was considered as the threshold resulting in the selection of one hit, compound **16**, which had its potential binding mode predicted by molecular docking (**Fig. 2b**). MST experiments to determine the K_D for the binding between compound **16** and HDAC6-EGFP WT were not possible to be performed considering the self-fluorescence displayed by ligand in concentrations higher than 100 µM. In addition to the positive binding control mono-Ub (ZnF-UBP-positive/catalytic-negative), the selective HDAC6 inhibitor tubastatin A (ZnF-UBP-negative/catalytic-positive binding control) and a class I-selective hydroxyl ketone inhibitor (HKI, ZnF-UBP-negative/catalytic-negative binding control, **Fig. S6**)[14] were probed. Binding of HDAC6 catalytic inhibitors to the full length HDAC6 could be detected in both thermophoresis alone and thermophoresis + T-Jump (**Fig. 2c**), but only at a concentration (100 µM) well above their nanomolar catalytic IC_{50}. Moreover, their T-Jump values alone (**Fig. 2d**) point to an

absence of binding close to the fluorophore (i.e. the ZnF-UBP), corroborating the use of MST thermophoresis + T-Jump for detecting binding to the HDAC6 ZnF-UBP domain.

Looking for small molecules able to bind the ZnF-UBP will not necessarily provide compounds able to disrupt the HDAC6-Ub PPI. In the interaction surface between two proteins, small-molecule-like binding pockets (the hotspots) are much smaller than the protein-protein interface.[15, 16] To check the ability of compound **16** to inhibit this specific PPI, and to confirm the screening results, an ELISA-based PPI competition assay was further developed and conducted with the 40 SBVS hits. In this specific assay, His-tag mono-Ub was immobilized on Nickel-coated 96-well plates. Tag-free mono-Ub (positive competition control) or tested compounds were incubated with recombinant HDAC6 WT and then added to the plates. The competition was evaluated by calculating the fraction of HDAC6 bound to immobilized His-tag mono-Ub, following recognition of the His_6-Ub-HDAC6 complex by an anti-HDAC6 primary antibody (**Fig. 3a**). Concentration-response competition curves were first determined for controls titrated with tag-free mono-Ub (**Fig. 3b**). Then, the screening was conducted with the SBVS hits (**Fig. 3c**). Compound **16** was confirmed to disrupt the HDAC6-Ub PPI. Interestingly, tubacin and tubastatin A also inhibited the PPI (**Fig. 3c**). Such inhibition corroborates the MST results observed with the catalytic deficient HDAC6. Taken together, these results confirm for the first time that changes in the HDAC6 catalytic domains directly inhibits the HDAC6-Ub PPI, most likely via an allosteric-like mechanism. This was further observed for SAHA, a pan-HDAC inhibitor, to a lesser extent. On the contrary, class I selective inhibitors such as CI-994 and HKI, had no or poor effect on the PPI activity of HDAC6 (**Fig. 3c**).

Compound **30** appeared as a second hit in the ELISA-based PPI competition assay, despite the absence interaction by MST measurements. Given that compounds interacting with the catalytic domains, such as tubastatin A and tubacin, were shown to affect HDAC6-Ub interaction, hits **16** and **30** (**Fig. S6**) were tested for HDAC6 deacetylase activity. No catalytic inhibition was observed in these assays. However, a 2-fold increase in substrate deacetylation was verified for compound **30** (**Table S2**), which opens up the discussion on the mechanisms of HDAC6-Ub inhibition, other than the orthosteric interaction with the HDAC6 ZnF-UBP.

The MST assay using lysates of cells expressing full-length HDAC6-EGFP fusion proteins allowed meaningful investigation of the HDAC6-Ub PPI interaction, showing, for the first time, the direct role of HDAC6 catalytic inhibition on HDAC6-Ub PPI. In combination with an ELISA-based PPI assay, the MST method showed a potential application in identifying HDAC6-Ub PPI inhibitors as promising chemical probes devoid of HDAC6 catalytic effect. Such probes constitute a key element to explore mechanisms involved in aggresome regulation by HDAC6, which are of interest in cancer, viral infection, neurological diseases, and immune disorders[1, 17]. By combining the MST assay with the ELISA-based PPI competition assay, we identified the first inhibitor (**16**, IC50 78 μM) able to disrupt HDAC6-Ub PPI as full-length protein partners. Overall, the MST method is useful in measuring the interaction of the HDAC6 ZnF-UBP with its molecular partners, from small molecules to proteins.

Methods

1. HEK 293 cell cultures, transfection, and cell lysates

HEK 293 cells (ATCC® CRL-1573™) were cultered in Dulbecco's Modified Eagle Medium (DMEM) with high glucose (Gibco™, ThermoScientific # 41965120), supplemented with 10% fetal bovine serum, 100 units/mL penicillin, 100 μg/mL streptomycin, and 1% non-essential amino acids. Cultures were kept in 75 cm^2 culture flasks (NUNC, Thermo Scientific) at 37 ºC in a 5% CO_2 incubator (HERAcell, Heraeus). Cells were transfected with pEGFP.N1-HDAC6, pEGFP.N1-HDAC6 DC, or pEGFP.N1-HDAC6.delta ZnF-UBP for 48 h. Cell lysates were prepared in radioimmunoprecipitation assay buffer (RIPA buffer, Sigma-Aldrich # R0278) containing protease inhibitor cocktail (SIGMA*FAST*™, Sigma-Aldrich # S8820). EGFP concentration in the lysates was measured by fluorescence in the Monolith NT.115 Instrument (MO-G008, LED power 60%, excitation 460-480 nm, and emission 515-530 nm) using recombinant GFP (rGFP) as a standard (Roche Diagnostic AG # 11814524001).

2. Antibodies, proteins, plasmids, and reagents

Antibodies: HDAC6 (D21B10) Rabbit mAb (# 7612), β-actin (8H10D10) Mouse mAb (# 3700), Anti-rabbit IgG (H+L) (DyLight™ 800 4X PEG Conjugate) (# 5151), Anti-mouse IgG (H+L) (DyLight™ 680 Conjugate) (#5470) (all from Cell Signaling Technology, Danvers, MA, USA), Anti-Ubiquitin antibody [EPR8830] Rabbit mAb (# 134953, abcam, Cambridge, UK). Goat monoclonal anti-rabbit IgG-FITC (#SC-2012) was purchased from Santa Cruz Biotechnology Proteins: Ubiquitin, human, recombinant (# BML-UW-0280), Ubiquitin, human, recombinant, His-tag (BML-UW8610), NEDD8, human, recombinant, His-tag (BML-UW9225), ISG15, human, recombinant, His-tag (BML-UW9335) (all from Enzo Life Sciences, Inc.), GST-HDAC6, human, recombinant (Sigma-Aldrich, # SRP0108). Plasmids: pEGFP.N1-HDAC6, pEGFP.N1-HDAC6.DC, and pEGFP.N1-HDAC6.delta ZnF-UBP were a gift from Tso-Pang Yao (Addgene plasmids # 36188, 36189, and 36190, respectively)[18]. Reagents: Fluor de Lys® SIRT1 substrate (BML-KI177), Fluor de Lys® HDAC developer II (BML-KI176) (all from Enzo Life Sciences, Inc.), trichostatin A (Sigma-Aldrich, #T8552), tubastatin A (Apex Bio, #A410), tubacin (Sigma-Aldrich, # SML0065), SAHA (Sigma-Aldrich, # SML0061), CI-994 (Sigma-Aldrich, # C0621). The class I-selective hydroxyl ketone compound was a gift from Dr. Yung-Sing Wong[14]. All compounds screened for ZnF-UBP-Ub modulation were purchased from the Specs company (http//www.specs.net).

3. Ubiquitin chains

K48- and K63-linked ubiquitin chains were synthesized as previously described[19], using linkage-specific enzymes to catalyze the reactions. The mammalian enzyme E2-25K was used in the synthesis of K48-linked chains while the yeast complex Mms2/Ubc13 was used to synthesize K63-linked chains. To generate di-Ub chains, the Ub moiety forming the proximal end carried unmodified K48 or K63 and an extra C-terminal residue (D77). The Ub moiety forming the distal end carried unmodified C-terminal G76 and K48C or K63C mutants. After synthesis of Ub-chains, the extra C-terminal

residue in the proximal end was removed through reaction with a ubiquitin C-terminal hydrolase (UCH) enzyme. K48-, and K63-linked tetra-Ub chains were later synthesized by successive rounds of deblocking and conjugation.

4. SDS-page and immunoblotting

Lysates of HEK 293 cells overexpressing the EGFP fusion proteins were diluted 1:1 with sample buffer (240 mM Tris/HCl pH 6.8 containing 0.04% bromophenol blue, 40% glycerol with or without 200 mM DTT), heated at 70 ºC for 10 min, and separated on 8% polyacrylamide gel. Before binding experiments, lysates of HEK 293 cells were incubated with mono-Ub or Ub-chains (K48-linked di- and tetra-Ub, and K63-linked di- and tetra-Ub) and monitored by SDS-page and immunoblotting to test for chain degradation by deubiquitinating enzymes (DUBs) possibly present in the cell lysates. Lysates (2- to 4-fold dilution) were pre-incubated with 4 µM Ubiquitin aldehyde (Ubal; K48- and K63-linked Ub chains) and 4 mM 1,10-phenanthroline (1,10-phen; K63-linked Ub chains only) for 15 min at 37 ºC, followed by incubation with K63- or K48-linked Ub chains, for 10 min at 37 ºC. Samples were then diluted 1:1 with sample buffer, incubated for 20 min at room temperature, and separated on 15% polyacrylamide gel.

For immunoblotting, proteins were transferred on PVDF membranes, and the membranes were subsequently blocked with TBS containing dried-milk powder (5%) and Tween®-20 (0.05%) for 1 h at 4 ºC. Membranes were then incubated with primary antibodies, diluted 1:1000 (anti-HDAC6 and anti-Ub rabbit monoclonal) or 1:5000 (anti-β-actin mouse monoclonal) in TBS containing dried-milk powder (1%) and Tween®-20 (0.05%), overnight at 4 ºC. Membranes were washed three times with TBS containing Tween®-20 (0.05%) and incubated with secondary antibodies diluted 1:10000 in TBS containing dried-milk powder (1%) and Tween®-20 (0.05%) for 1 h at room temperature. Membranes were washed as previously described, and the results of immunoblotting were visualized with the Odyssey infrared imaging system (LI-COR Biosciences).

5. Structure-based virtual screening (SBVS)

Specs compounds were prepared for SBVS as previously described[20]. Briefly, the compounds were downloaded from the Specs website (www.specs.net, SC_specs_10 mg_May2013) and protonated at pH 7.4 using the Protonate 3D tool of MOE 2013.08 (Chemical Computing Group CCG, Montreal, Canada), followed by energy minimization (MOE, MMFF94x force field, R-field equation for solvation, and 0.1 kcal/mol/Å2 as RMS gradient cut-off). Raccoon v1.0[21] was used to convert the ligand input files to the .pdbqt format. Atomic coordinates for HDAC6 ZnF-UBP (PDB 3GV4) were retrieved from the Protein Data Bank (http://www.wwpdb.org/). Protein structure was prepared using the AutoDock Tools (ADT) module of MGLTools v1.5.6[22]. The co-crystallized ubiquitin C-terminal peptide RLRGG and water molecules were removed from the protein structure, followed by the addition of Gasteiger charges and non-polar hydrogens. The binding site was centered on the carboxyl group of the C-terminal glycine in the co-crystallized peptide RLRGG. Box dimensions were 20 x 18 x 20 Å. Docking calculations were performed with AutoDock Vina[23] using default parameters. 20 binding poses were generated for each compound. The best-ranked compounds with scores < -8.5 kcal/mol were further filtered for solubility (> 100 µM) and logP (< 5.0), as predicted with VolSurf + version 1.0.7[24], resulting in 609 compounds that were visually inspected to ensure proper fit to the Ub binding pocket. 80 ligands were selected for re-docking in HDAC6 ZnF-UBP using GOLD version 5.2 (CCDC, Cambridge, UK). The binding site was defined within a 6 Å radius around the co-crystallized peptide. 100 docking poses were generated for each Specs compound, by using 100,000 GOLD Genetic Algorithm interactions (Preset option), and ranked according to the ChemPLP score. Finally, 40 compounds with a ChemPLP score higher than 70 were selected for *in vitro* binding experiments.

6. Microscale thermophoresis (MST)

Solutions and serial dilutions of non-tagged mono-Ub, K48-linked di-Ub, and K63-linked di- and tetra-Ub were prepared in 50 mM Tris/HCl buffer pH 8.0 containing 150 mM NaCl while solutions of K48-linked tetra-Ub (K48C mutation in the distal Ub moiety) were prepared in this same buffer supplied with 5 mM DTT. Solutions and serial dilutions of His-tag mono-Ub, NEDD8, and ISG15 were prepared in 20 mM Hepes pH 8.0 containing 50 mM NaCl and 1 mM DTT. Lysates of HEK 293 cells overexpressing EGFP-HDAC6 wild type (WT), EGFP-HDAC6 catalytic deficient (CD), and EGFP-HDAC6 ΔZnF-UBP were used as source of labeled fluorescent proteins for MST experiments. In addition, control experiments were performed for non-tagged mono-Ub labeled with the fluorescent dye NT-647 (Monolith NT^{TM} Protein Labeling Kit RED-NHS, NanoTemper Technologies GmbH, München, Germany) and purified GST-HDAC6 WT (**Fig. S7)**. Protein concentrations of unlabeled mono-Ub, Ub chains, Ub-like proteins, and GST-HDAC6 stock solutions were measured using the Qubit® Protein Assay (ThermoFisher Scientific, # Q33211).

Protein-protein interactions between HDAC6 and mono-Ub were first evaluated by microscale MST for the isolated protein partners: fluorescent labeled non-tagged mono-Ub and GST-HDAC6. To determine the dissociation constants, 10 µL of 132 nM labeled mono-Ub (50 mM Tris/HCl pH 8.0, 137 mM NaCl, 2.7 mM KCl, 1 mM $MgCl_2$, 1 mg/mL BSA) were mixed with 10 µL of unlabeled GST-HDAC6 WT in different concentrations ranging from 0.55 to 8931 nM (serial dilutions in 50 mM Tris/HCl pH 8.0, 137 mM NaCl, 2.7 mM KCl, 1 mM $MgCl_2$, 1 mg/mL BSA, 10% glycerol), and incubated for 15 min at room temperature. Samples were loaded into MST premium coated capillaries (NanoTemper Technologies GmbH, München, Germany, # MO-K005), and the thermophoresis of each concentration was measured at excitation 605-645 nm and emission 680-685 nm using the Monolith NT.115 (NanoTemper Technologies GmbH, München, Germany). Measurements were performed at room temperature for 30 s at 60% LED power and 40% infrared laser power (**Fig. S7**).

For MST experiments with tag-free mono-Ub and Ub chains (**Fig. S4**), lysates of cells expressing EGFP fusion proteins, diluted from 2- to 4-fold in lysis buffer, were pre-incubated with 4 µM Ubal alone (experiments with mono-Ub and K48-linked Ub chains), or 4 µM Ubal and 4 mM 1,10-phenanthroline (experiments with mono-Ub and K63-linked Ub chains), for 15 min at 37 ºC.

Subsequently, 10 µL of lysates were mixed with 10 µL of unlabeled mono-Ub or Ub chains solutions at different concentrations. These mixtures were incubated for 10 min at 37 ºC, samples were loaded into MST premium coated capillaries, and thermophoresis of each concentration was measured at excitation 460-480 nm and emission 515-530 nm using the Monolith NT.115. Lysates were tested in final dilutions between 4- and 8- fold (final EGFP concentrations of approximately 25 nM) while the final concentrations of Ubal and 1,10-phenanthroline were 2 µM and 2 mM, respectively. Each measurement was performed at room temperature for 30 s at 95% LED power and 40% infrared laser power. Experiments with His-tag mono-Ub and Ub-like proteins were performed according to the same protocol without pre-incubation with Ubal and 1,10-phenanthroline (1,10-phe). Concentrations of unlabeled proteins ranged from 0.70 to 60,000 nM. The dissociation constants were determined by the law of mass action Kd formula available on Monolith NT.115 data analysis tool. In addition, fraction bound values were calculated for each concentration by subtracting the baseline of each individual experiment and dividing by its amplitude. Fraction bound values were then fitted in GraphPad® Prism 7.0 using nonlinear regression: log (agonist) vs. response (three parameters).

The optimized MST assay was further applied to test the 40 compounds selected by SBVS for their binding to HDAC6. Briefly, 100 µM of the tested compounds were pre-incubated (10 min, 37 °C) with lysates of HEK293 cells expressing HDAC6-EGFP WT. MST measurements were performed at room temperature for 30 s at 95% LED power and 40% infrared laser power. MST curves for the tested compounds were compared to those obtained for unbound (lysate alone) and bound controls (lysates pre-incubated with 50 µM ubiquitin). Fraction bound values were determined for triplicate measurements by subtracting the baseline of the unbound control and dividing by the amplitude of the bound control (50 µM ubiquitin).

7. HDAC6 catalytic assay

In vitro HDAC6 activity was detected by measuring the fluorophore released from the Fluor de Lys® acetylated substrate upon deacetylase activity. Trichostatin A (a pan-HDAC inhibitor) was used as positive control. Stock solutions of trichostatin A and tested molecules in DMSO were diluted in

HDAC assay buffer (50 mM Tris/HCl pH 8.0, 137 mM NaCl, 2.7 mM KCl, 1 mM $MgCl_2$, 1 mg/mL BSA). The final DMSO concentration was kept at 2%. For each tested concentration, a corresponding blank was included to detect self-fluorescence artefacts. Assays were conducted in duplicate in 96-well plates at 37 °C for 1h. Enzymatic reactions were stopped by adding HDAC developer II followed by 3 h incubation at RT. The resulting fluorescence intensity was measured at 360 nm excitation and 460 nm emission, using a FLx800 microplate reader (Biotek®). Untreated enzyme wells were included in each experiment as the 100% deacetylase activity control. IC_{50} values were determined through titration with the tested compounds and data was fitted in a concentration response model using GraphPad® Prism 7.0.

A mass spectrometry-based assay was used to evaluate the deacetylase activity of the fusion HDAC6-EGFP proteins in lysates of HEK 293 cells. Briefly, 10.5 µM of the selective HDAC6 substrate BATCP (Sigma-Aldrich) was added to the lysates (dilution 1:1 v/v, resulting in final HDAC6-concentrations of 50, 25, and 12.5 nM). Reactions were incubated at 37°C for 4 h and then stopped by the addition of cold acetonitrile. The plate was kept at -80°C for 10 min and then centrifuged at 5000 x *g* for 10 min. Supernatants were transferred into UHPLC-compatible 96-well plates to be analyzed on a UHPLC-ESI-MS/MS system consisting of an Acquity UPLC System (Waters, Milford, MA, USA) connected to a Quattro Micro triple quadrupole mass spectrometer equipped with an ESI source operating in positive-ion mode (Waters). Deacetylase activity was determined as previously described[25].

8. ELISA-based PPI competition assay

His-tag ubiquitin was prepared at 1 µM in BupH™ Tris Buffer (Thermo Scientific, pH = 7.2) and immobilized on Pierce® Nickel coated 96-wells plates (Thermo Scientific) overnight (100 µl/well) at room temperature (RT). Plates were then washed 3x (wash buffer A: 25 mM Tris/HCl pH 7.2, 150 mM NaCl, 0.05% Tween-20). Recombinant HDAC6 WT (0.2 µM, 2% DMSO in HDAC6 assay buffer) was used as bound control (HDAC6, 100% binding to His_6-Ub) while a pre-incubated mixture containing 0.1 µM HDAC6, 0.05-150 µM tag-free mono-Ub and 2% DMSO (HDAC6/tag-free Ub)

was used as competition control. For test compounds, a pre-incubated mixture of HDAC6, 100 µM compound and 2% DMSO (HDAC6/compound) was used. Solutions of HDAC6 (for bound control and blank), HDAC6/tag-free Ub (for competition control) or HDAC6/compound (for test) were added to wells containing immobilized His_6-Ub. Plates were then incubated for 1 h at room temperature (RT) and washed once (wash buffer B: 50 mM Tris/HCl pH 8.1, 137 mM NaCl, 1 mM $MgCl_2$, 2.7 mM KCl, 0.05% Tween-20). Anti-HDAC6 primary rabbit antibody (1:400) was added to control and test wells, while half of the wells that contained HDAC6 alone were considered as blanks and received HDAC6 assay buffer instead, and the plate was incubated overnight at RT. Wells were washed three times (wash buffer B), followed by incubation with an anti-rabbit IgG-FITC secondary antibody (1:200) for 2 h at RT. Finally, wells were washed three times (wash buffer B) and 100 µL of HDAC6 assay buffer was added to blank, sample and controls wells prior to fluorescence measurements on a FLx800 microplate reader (BioTek®, excitation at 485/20 nm and emission at 528/20 nm). PPI inhibition was calculated in terms of HDAC6 fraction bound to His_6-Ub, using the competition control (tag-free Ub) at 50 µM as the unbound reference. IC_{50} values were determined for concentration-response curves titrated with tag-free mono-Ub (competition control) and tested molecules. Competition data were plotted and fitted in GraphPad® Prism 7.0.

Aknowledgements

Authors are thankful to the Swiss National Science Foundation (P300P3_158507) and Pierre Mercier Foundation (Switzerland) for financial support.

References

1. Falkenberg, K.J. & Johnstone, R.W. Histone deacetylases and their inhibitors in cancer, neurological diseases and immune disorders. *Nat Rev Drug Discov* **13**, 673-691 (2014).
2. Catley, L. *et al.* Aggresome induction by proteasome inhibitor bortezomib and alpha-tubulin hyperacetylation by tubulin deacetylase (TDAC) inhibitor LBH589 are synergistic in myeloma cells. *Blood* **108**, 3441-3449 (2006).
3. Hideshima, T., Richardson, P.G. & Anderson, K.C. Mechanism of action of proteasome inhibitors and deacetylase inhibitors and the biological basis of synergy in multiple myeloma. *Mol Cancer Therap* **10**, 2034-2042 (2011).
4. Simões-Pires, C.A., Bertrand, P. & Cuendet, M. Novel histone deacetylase 6 (HDAC6) selective inhibitors: a patent evaluation (WO2014181137). *Expert Opin Ther Pat* **27**, 229-236 (2017).
5. Boyault, C., Sadoul, K., Pabion, M. & Khochbin, S. HDAC6, at the crossroads between cytoskeleton and cell signaling by acetylation and ubiquitination. *Oncogene* **26**, 5468-5476 (2007).
6. Kawaguchi, Y. *et al.* The deacetylase HDAC6 regulates aggresome formation and cell viability in response to misfolded protein stress. *Cell* **115**, 727-738 (2003).
7. Hao, R. *et al.* Proteasomes activate aggresome disassembly and clearance by producing unanchored ubiquitin chains. *Mol Cell* **51**, 819-828 (2013).
8. Li, Z.-y. *et al.* A novel HDAC6 inhibitor Tubastatin A: Controls HDAC6-p97/VCP-mediated ubiquitination-autophagy turnover and reverses temozolomide-induced ER stress-tolerance in GBM cells. *Cancer Lett* **391**, 89-99 (2017).
9. Ouyang, H. *et al.* Protein aggregates are recruited to aggresome by histone deacetylase 6 via unanchored ubiquitin C termini. *J Biol Chem* **287**, 2317-2327 (2012).
10. Harding, R.J. *et al.* Small molecule antagonists of the interaction between the histone deacetylase 6 zinc-finger domain and ubiquitin. *J Med Chem* (2017). doi: 10.1021/acs.jmedchem.7b00933
11. Jerabek-Willemsen, M. *et al.* MicroScale Thermophoresis: Interaction analysis and beyond. *J Mol Struct* **1077**, 101-113 (2014).
12. Boyault, C. *et al.* HDAC6-p97/VCP controlled polyubiquitin chain turnover. *Embo J* **25**, 3357-3366 (2006).
13. Dos Santos Passos, C., Simões-Pires, C.A., Carrupt, P.A. & Nurisso, A. Molecular dynamics of zinc-finger ubiquitin binding domains: a comparative study of histone deacetylase 6 and ubiquitin-specific protease 5. *J Biomol Struct Dyn* **34**, 2581-2598 (2016).
14. Traoré, M.D.M. *et al.* Hydroxyl Ketone-Based Histone Deacetylase Inhibitors To Gain Insight into Class I HDAC Selectivity versus That of HDAC6. *ACS Omega* **2**, 1550-1562 (2017).
15. Arkin, M.R. & Wells, J.A. Small-molecule inhibitors of protein-protein interactions: progressing towards the dream. *Nat Rev Drug Discov* **3**, 301-317 (2004).
16. Scott, D.E., Bayly, A.R., Abell, C. & Skidmore, J. Small molecules, big targets: drug discovery faces the protein-protein interaction challenge. *Nat Rev Drug Discov* **15**, 533-550 (2016).
17. Banerjee, I. *et al.* Influenza A virus uses the aggresome processing machinery for host cell entry. *Science* **346**, 473-477 (2014).
18. Gao, Y.S., Hubbert, C.C. & Yao, T.P. The microtubule-associated histone deacetylase 6 (HDAC6) regulates epidermal growth factor receptor (EGFR) endocytic trafficking and degradation. *J Biol Chem* **285**, 11219-11226 (2010).
19. Pickart, C.M. & Raasi, S. Controlled synthesis of polyubiquitin chains. *Methods Enzymol* **399**, 21-36 (2005).
20. Sacconnay, L. *et al.* 5-Benzylidene-hydantoin is a new scaffold for SIRT inhibition: From virtual screening to activity assays. *Eur J Pharm Sci* **85**, 59-67 (2016).
21. Forli, S. *et al.* Computational protein-ligand docking and virtual drug screening with the AutoDock suite. *Nat Protoc* **11**, 905-919 (2016).

22. Morris, G.M. *et al.* AutoDock4 and AutoDockTools4: Automated docking with selective receptor flexibility. *J Comput Chem* **30**, 2785-2791 (2009).
23. Trott, O. & Olson, A.J. AutoDock Vina: improving the speed and accuracy of docking with a new scoring function, efficient optimization and multithreading. *J Comput Chem* **31**, 455-461 (2010).
24. Cruciani, G., Crivori, P., Carrupt, P.A. & Testa, B. Molecular fields in quantitative structure–permeation relationships: the VolSurf approach. *J Mol Struct THEOCHEM* **503**, 17-30 (2000).
25. Zwick, V., Simões-Pires, C. & Cuendet, M. Cell-based multi-substrate assay coupled to UHPLC-ESI-MS/MS for a quick identification of class-specific HDAC inhibitors. *J Enzyme Inhib Med Chem* **31**, 209-214 (2016).

Figures

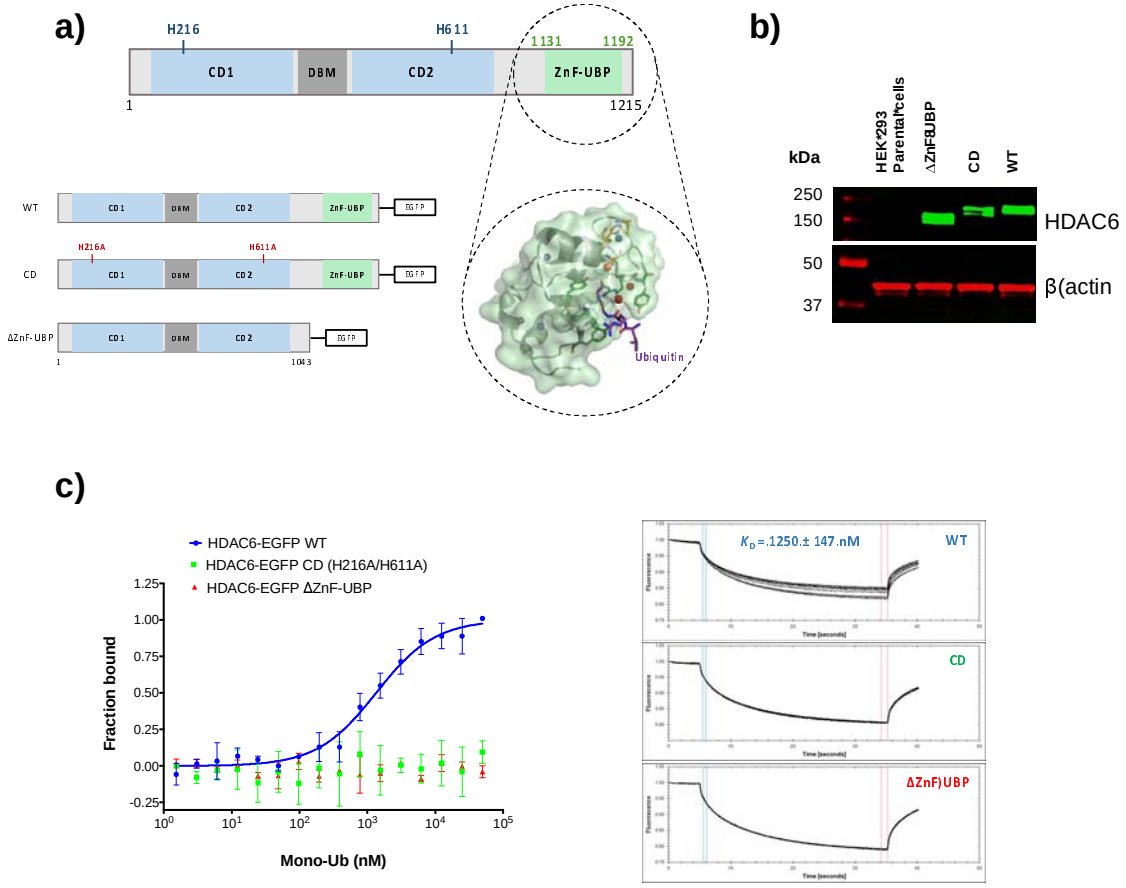

Fig. 1. Overexpression of HDAC6-EGFP fusion proteins in HEK 293 cells and their interaction with recombinant mono-Ub measured by MST. a) Scheme of the full length HDAC6 depicting its catalytic domains (CD1, CD2) and the zinc-finger ubiquitin binding domain (ZnF-UBP) able to recognize the C-terminal GG motif of Ubiquitin (Ub). Detail: molecular surface of HDAC6 ZnF-UBP in complex with Ub C-terminus RLRGG (sticks). Image generated with MOE 2015.10 from PDB: 3GV4. **b)** Western blot analysis of cell lysates from HEK 293 cells overexpressing HDAC6-EGFP fusion proteins: wild-type (HDAC6-EGFP WT), catalytic deficient (HDAC6-EGFP CD), and ZnF-UBP deleted (HDAC6-EGFP ΔZnF-UBP). **c)** MST titration binding experiments showing the interaction between HDAC6-EGFP WT fusion protein and mono-Ub, and the absence of interaction between HDAC6-EGFP CD / ΔZnF-UBP and mono-Ub.

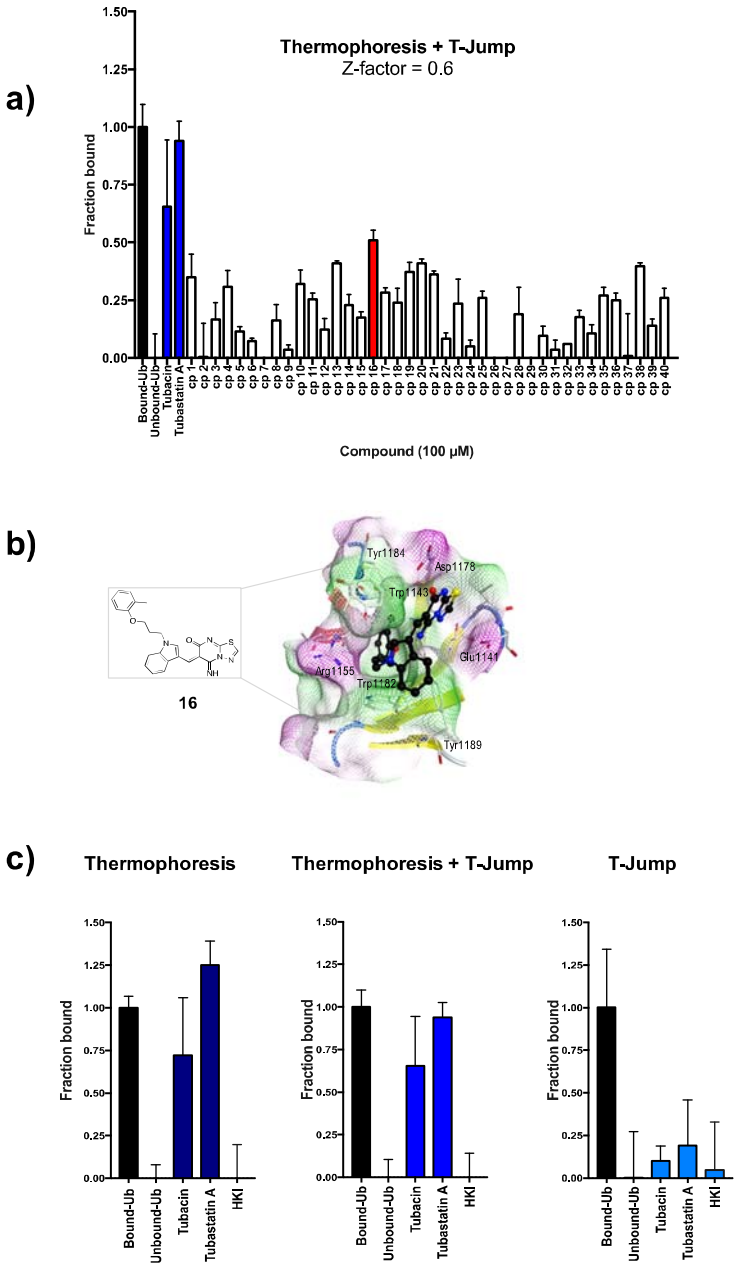

Fig. 2. Microscale thermophoresis (MST) applied for the screening of HDAC6 ligands: detection of binding on both catalytic and ZnF-UBP domains. a) Selected compounds were screened at 100 µM. Fraction bound values were obtained by normalizing the amplitude of thermophoresis + T-Jump values (between 100 and 0 µM compound) over the amplitude values between bound (50 µM mono-Ub) and unbound (0 µM mono-Ub) controls. **b)** Best ranked docking pose for compound **16** in complex with HDAC6 ZnF-UBP. Compound **16** is represented as balls & sticks. 2D structure is also depicted. The molecular surface around the ligand is color-coded based on lipophilicity (green: hydrophobic; purple: hydrophilic). Key amino acids surrounding **16** are labelled in black. Image was generated with MOE 2015.10. **c)** Comparison of MST measurements with HDAC6-selective deacetylase inhibitors tested at 100 µM: T-Jump analysis detects preferentially binding close to the fluorophore (EGFP is fused to the C-terminus of HDAC6) and to a lesser extent the binding of catalytic inhibitors.

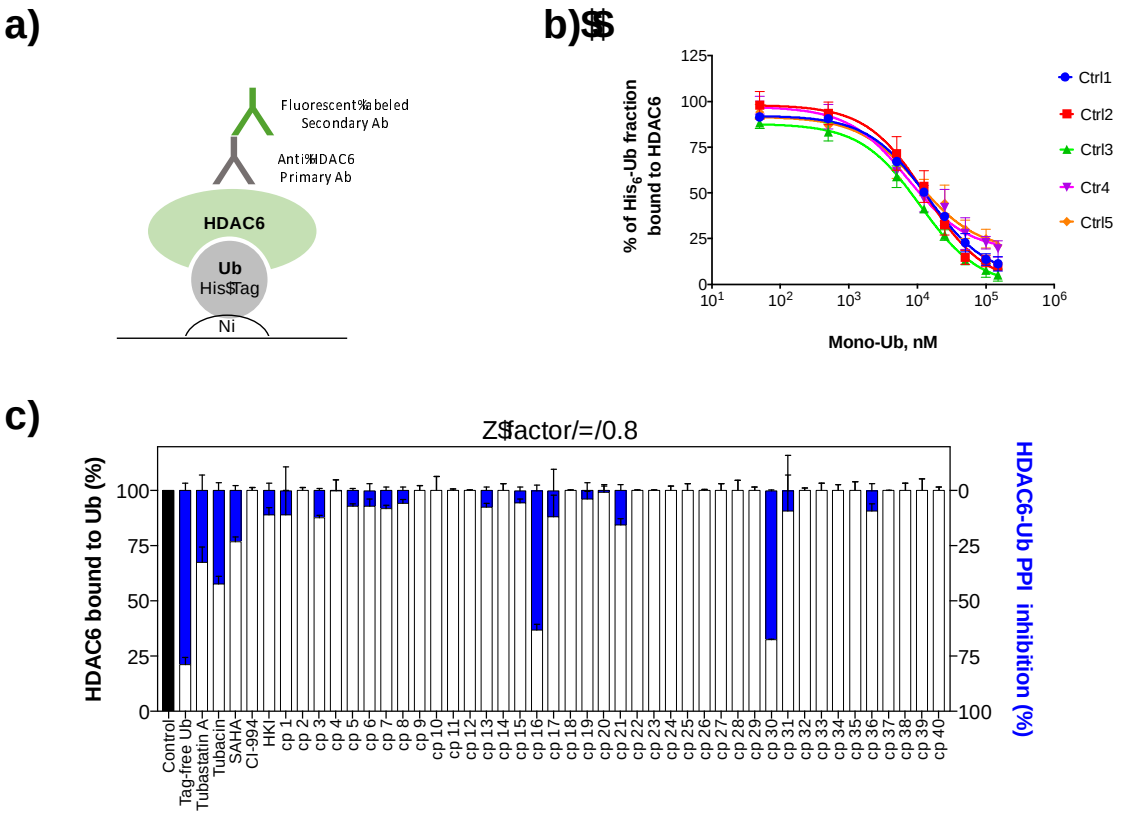

Fig. 3. ELISA-based method for measuring the inhibition of the protein-protein interaction (PPI) between HDAC6 and Ub. a) His_6-Ub was immobilized on Nickel (Ni) coated 96-wells plates and let to interact with recombinant HDAC6 WT. After washing steps to remove unbound proteins and ligands, plates were subjected to sequential incubations and washing with an anti-HDAC6 antibody and a fluorescent labeled secondary antibody. HDAC6 interaction with immobilized His_6-Ub was detected by fluorescence measurements. **b)** Control experiments were performed to evaluated whether tag free mono-Ub could compete with immobilized His_6-Ub for its binding to HDAC6. Competition curves from five independent experiments showed that pre-incubation of HDAC6 with increasing concentrations of tag free mono-Ub reduced the His_6-Ub-HDAC6 complex formation in a concentration-dependent fashion (IC_{50} = 11,157 ± 2665 nM). **c)** Screening of 40 selected SPECS compounds for HDAC6-Ub PPI inhibition by the ELISA-based method.

Supplementary Information

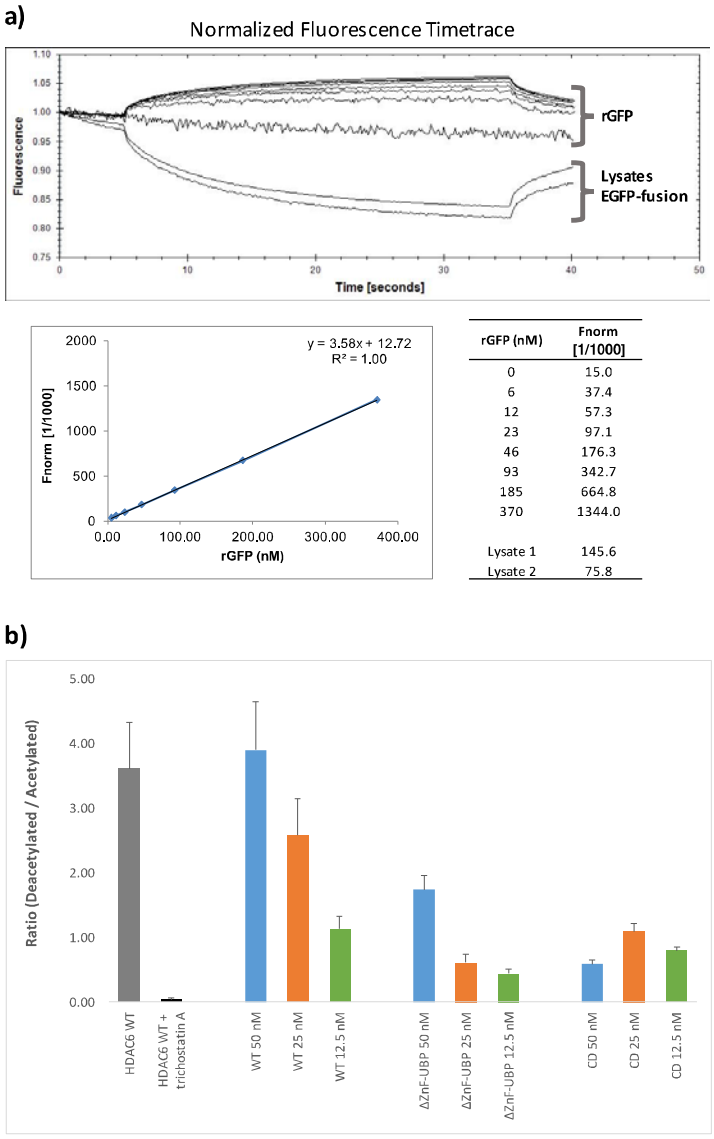

rGFP (nM)	Fnorm [1/1000]
0	15.0
6	37.4
12	57.3
23	97.1
46	176.3
93	342.7
185	664.8
370	1344.0
Lysate 1	145.6
Lysate 2	75.8

Fig. S1. (A) Calibration curve for recombinant GFP (rGFP). Fluorescence of rGFP and of the EGFP-fusion proteins in the cell lysates was measured in the Monolith NT.115 Instrument (LED power 60%, excitation 460-480 nm, and emission 515-530 nm). (B) MS-based catalytic activity of HDAC6-EGFP fusion proteins in lysates of transfected HEK 293 cells. The deacetylase activity of EGFP-fusion proteins in the lysates was measured using the HDAC6 selective substrate BATCP according to described by Zwick et al. (2016)[1]. Lysates were diluted to result in final EGFP concentrations of 50, 25, and 12.5 nM, corresponding to the concentrations of HDAC6-EGFP fusion proteins used for the MST measurements. Deacetylase activity of recombinant HDAC6 WT (50 U/well, Sigma-Aldrich) was measured as control in presence and absence of the pan-HDAC inhibitor trichostatin A (300 nM). Lysates of cells expressing HDAC6-ΔZnF-UBP showed a decrease in deacetylase activity in comparison with HDAC6 WT. On the other hand, the deacetylase activity observed for lysates of cells expressing HDAC6 CD is probably due to basal HDAC6 in HEK 293 cells.

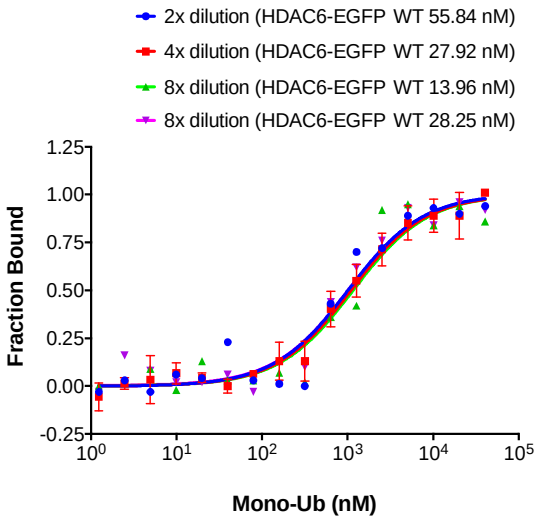

	K_D (nM)
Batch 2 (1 experiment) **2-fold dilution** 56 nM HDAC6-EGFP WT	980
Batch 1 (2 experiments) **4-fold dilution** 25 nM HDAC6-EGFP WT	1250 ± 147
Batch 2 (1 experiment) **4-fold dilution** 28 nM HDAC6-EGFP WT	
Batch 2 (1 experiment) **8-fold dilution** 14 nM HDAC6-EGFP WT	1170
Batch 3 (1 experiment) **8-fold dilution** 28 nM HDAC6-EGFP WT	998

Fig. S2. MST experiments with different batches of lysates diluted 2-, 4- and 8-fold indicated no significant competition between recombinant mono-ubiquitin and endogenous free ubiquitin or other Ub-like proteins. Binding curves for batches 1 (25 nM HDAC6-EGFP WT, 4-fold dilution) and 2 (28 nM HDAC6-EGFP-WT, 4-fold dilution) are the same presented in Fig 1c.

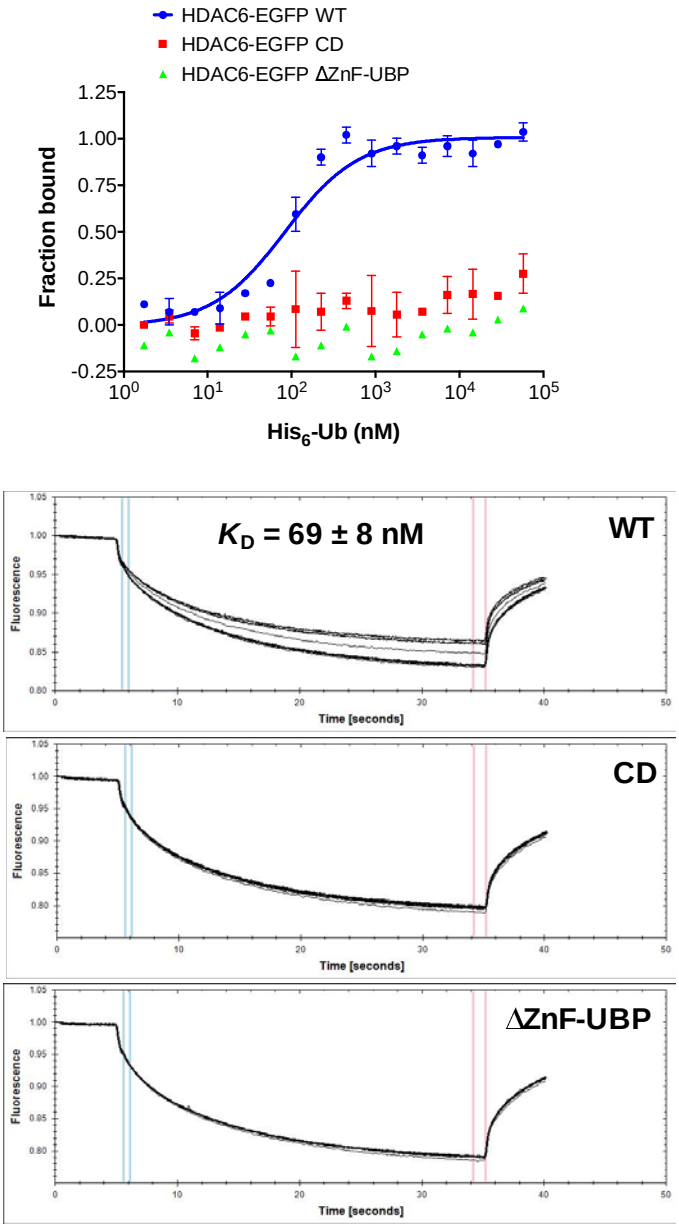

Fig. S3. MST binding experiments with HDAC6-EGFP fusion proteins in lysates of HEK 293 cells and His_6-ubiquitin (His_6-Ub). Lysates of cells expressing HDAC6-EGFP WT, CD, and ΔZnF-UBP were diluted to result in EGFP final concentrations corresponding to approximately 25 nM. As observed for non-tagged mono-Ub, His_6-Ub showed to interact with HDAC6-EGFP WT but not with HDAC6-EGFP CD or HDAC6 EGFP-ΔZnF-UBP. The K_D of 69 nM indicates that His_6-Ub binds to HDAC6 with approximately 20-fold higher affinity than non-tagged mono-Ub. This binding affinity is close to the K_D reported for the binding between HDAC6 ZnF-UBP and His_6-Ub (K_D = 60 nM, measured by isothermal titration calorimetry)[2].

a)

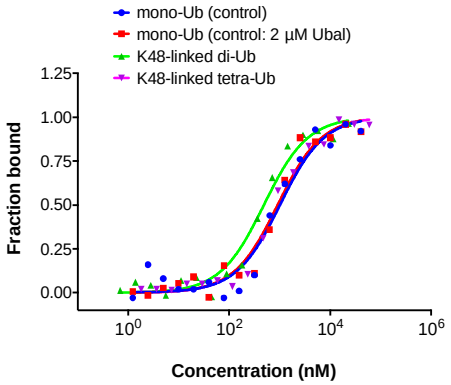

	K_D (nM)
(ctrl 1) mono-Ub	998 ± 81
(ctrl 2) mono-Ub 2 µM Ubal	900 ± 91
K48-linked di-Ub	474 ± 63
K48-linked tetra-Ub	916 ± 104

b)

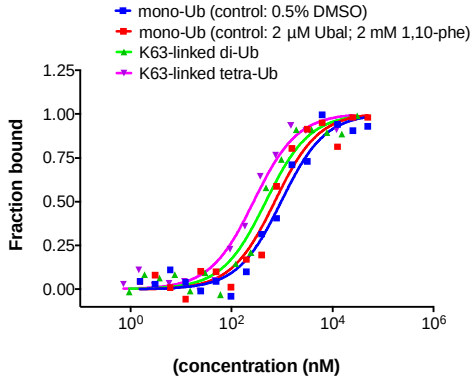

	K_D (nM)
(ctrl 1) mono-Ub 0.5% DMSO	946 ± 161
(ctrl 2) mono-Ub 2 µM Ubal 2 mM 1,10-phe	687 ± 99
K63-linked di-Ub	467 ± 99
K63-linked tetra-Ub	258 ± 37

c)

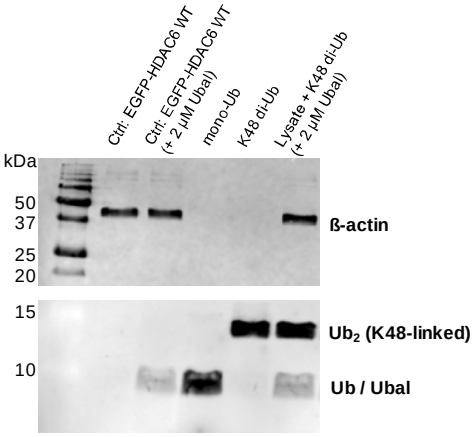

d)

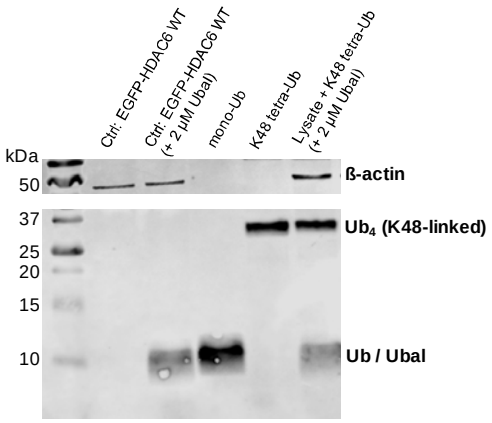

e)

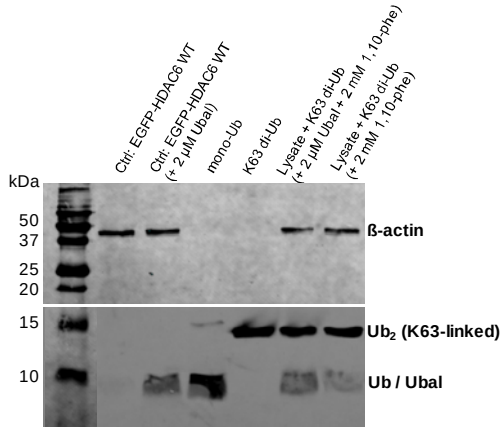

f)

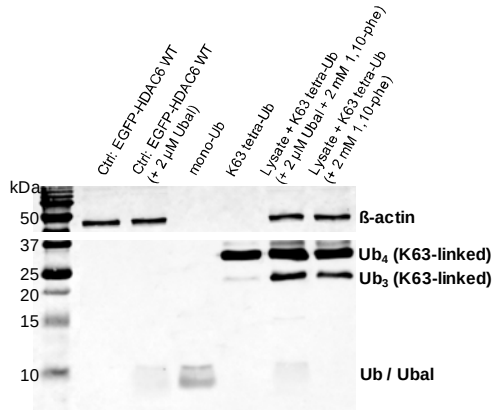

Fig. S4. HDAC6-EGFP WT binds to mono-ubiquitin, K48-, and K63-linked polyubiquitin chains with similar affinities. To avoid degradation by endogenous deubiquitinating enzymes (DUBs), lysates were pre-incubated with 2 µM ubiquitin aldehyde (Ubal) for experiments with K48-linked polyubiquitin chains and with 2 µM Ubal + 2 mM 1,10-phenanthroline for experiments with K63-polyubiquitin chains[3]. (A) MST data for mono-ubiquitin and K48-linked polyubiquitin chains binding to HDAC6-EGFP WT. (B) MST data for mono-ubiquitin and K63-linked polyubiquitin chains binding to EGFP-HDAC6 WT. The observed 2-fold higher affinity measured for K48- and K63-linked di-Ub as well as the 4-fold higher affinity measured for K63-linked tetra-Ub may indicate some DUB activity in the lysates. To address this possibility, we verified the integrity of K48- and K63-linked polyubiquitin after their incubation with lysates of cells expressing the HDAC6-EGFP fusion proteins under the same conditions used in the binding assays. Lysates pre-incubated with 2 µM Ubal (15 min, 37 ºC) were further incubated with (C) 10 µM K48-linked di-Ub (10 min, 37 °C) or (D) 10 µM K48-linked tetra-Ub (10 min, 37 °C), and chain integrity was analyzed by western blot. Lysates pre-incubated with 2 µM Ubal + 2 mM 1,10-phenanthroline or with 1,10-phenanthroline alone (15 min, 37 ºC) were incubated with (E) 10 µM K63-linked di-Ub (10 min, 37 °C) or (F) 10 µM K63-linked tetra-Ub (10 min, 37 °C) and analyzed by western blot. Control experiments were performed with 10 µM mono-Ub or polyubiquitin chains incubated with lysis buffer. These data showed that polyubiquitin chains can be degraded by DUBs present in the lysates even after a pre-incubation step with DUB inhibitors indicating a drawback for the proposed method.

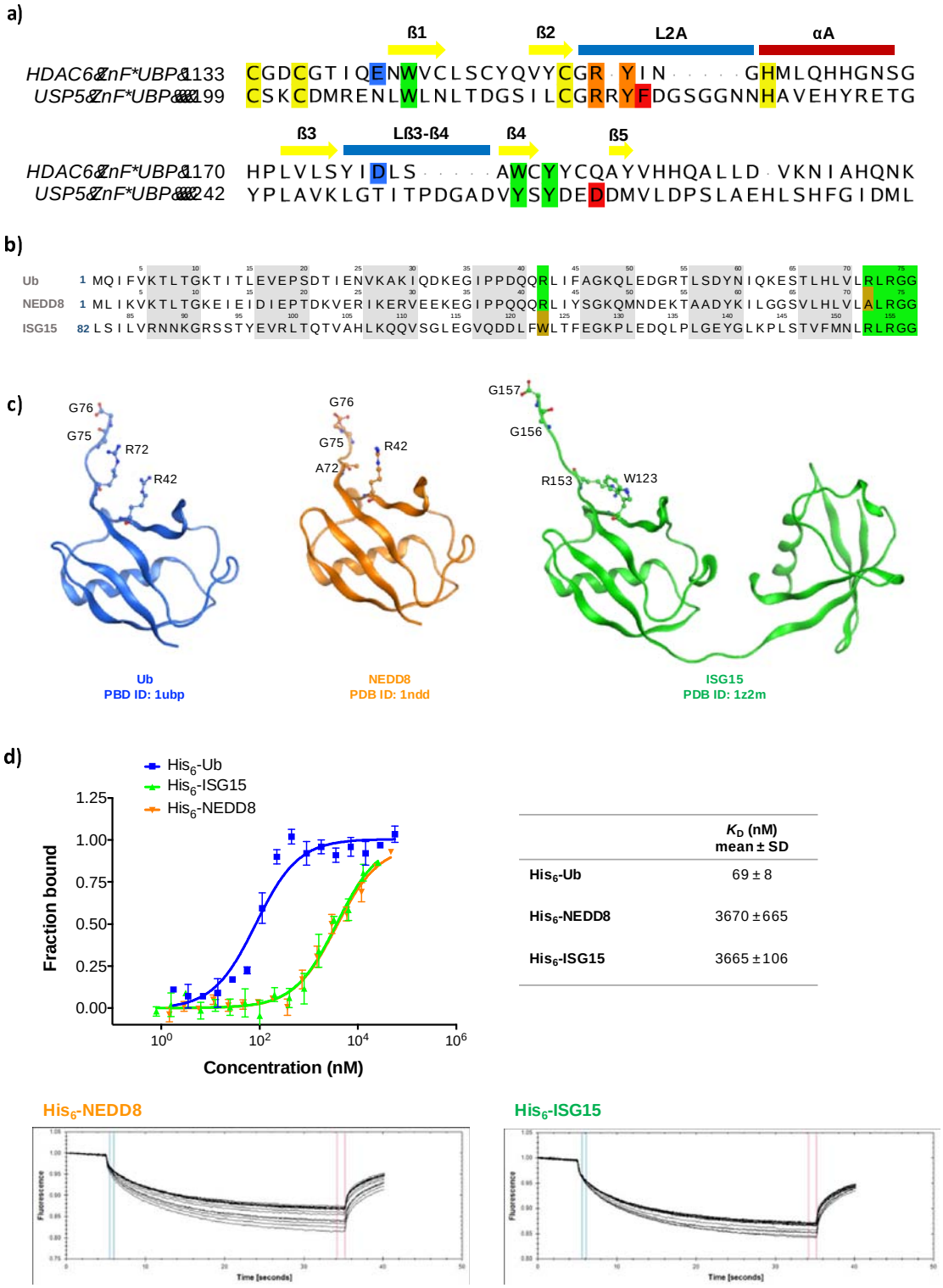

Fig. S5. Mono-ubiquitin binds to EGFP-HDAC6 WT with 50-fold higher affinity than the ubiquitin-like proteins NEDD8 and ISG15. (A) Sequences of HDAC6 ZnF-UBP and USP5 ZnF-UBP. Residues coordinating with Zn^{2+} are highlighted in yellow and residues interacting with ubiquitin are highlighted in green (aromatic pocket), orange (loop L2A), blue (HDAC6 residues non-conserved in USP5), and red (USP5 residues non-conserved in HDAC6)[4]. (B) Sequence alignment of

human ubiquitin (Uniprot ID: P0GC48, residues 1-76) with the mature forms of human NEDD8 (Unipoprot ID: Q15843, residues 1-76) and ISG15 (Uniprot ID: P05161, residues 82-157). Conserved residues contributing to HDAC6-ubiquitin binding are highlighted in green. Non-conserved NEDD8 A72 and ISG15 W123 residues are highlighted in dark yellow. (C) 3D structures of human ubiquitin, NEDD8, and ISG15. (D) MST data for His_6-NEDD8 and His_6-ISG15 binding to HDAC6-EGFP WT. Curve for His_6-Ub binding to HDAC6-EGFP is the same presented in **Figure S3**.

In summary, we observed that neither mono-ubiquitin or the ubiquitin-like proteins NEDD8 and ISG15 could bind HDAC6-EGFP ΔZnF-UBP (data not shown), confirming that the ZnF-UBP domain is essential for their interactions with HDAC6. In addition, these results support our previous molecular dynamics data suggesting that ubiquitin R42 and R72 may contribute to HDAC6-Ub binding by interacting with HDAC6 E1141 and D1178[4].

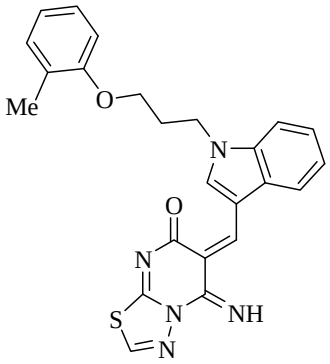

Compound 16
AN-758/41576910

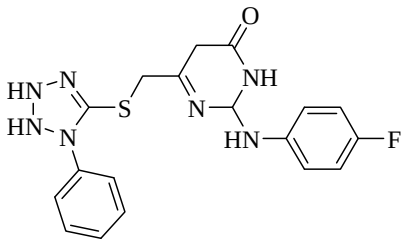

Compound 30
AJ-292/42490180

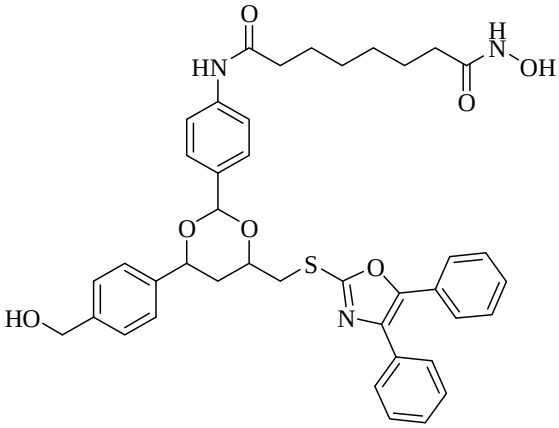

Tubacin

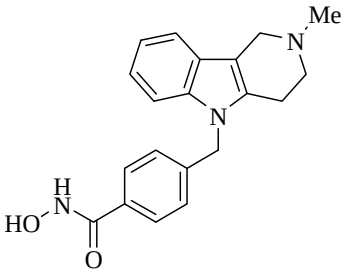

Tubastatin A

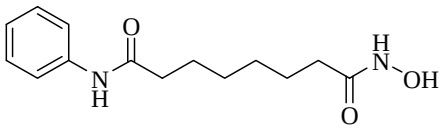

SAHA

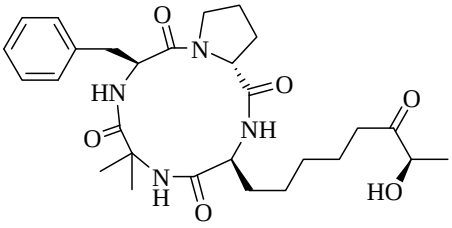

HKI

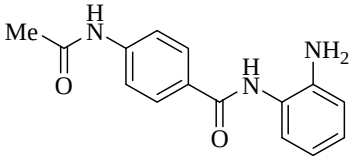

CI-994

Fig. S6. 2D structures of biologically active compounds (16 and 30) selected from SBVS and positive/negative controls. Compound **16** was a hit at 100 μM in the MST screening assay for binding full-length HDAC6 and was able to inhibit HDAC6-Ub PPI in the ELISA-based assay (IC_{50}=78 μM). Compound **30** was shown to inhibit the HDAC6-Ub PPI in the ELISA-based assay (IC_{50}=95 μM). Tubacin and Tubastatin A are known catalytic inhibitors selective to HDAC6. HKI and CI-994 are selective inhibitors of class I (nuclear) HDACs.

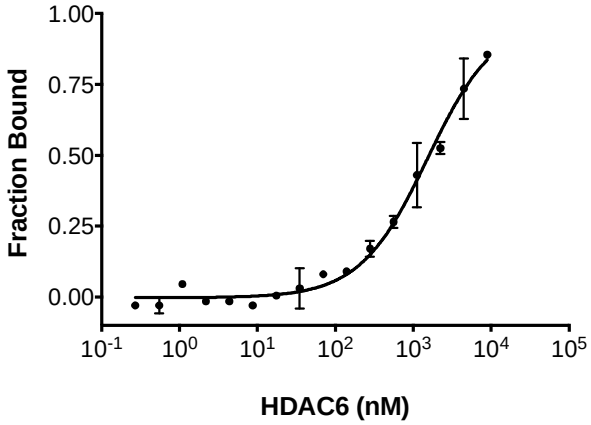

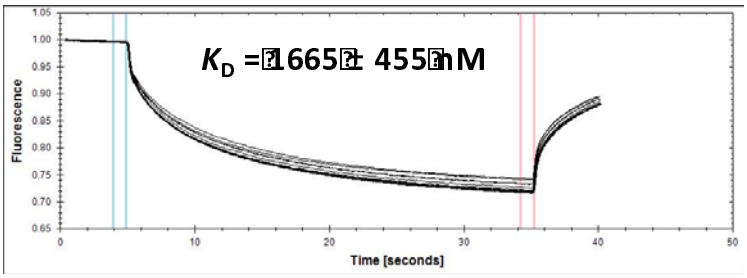

Fig. S7. Binding of recombinant full length HDAC6 WT to mono-Ub labeled with NT-647 using NHS coupling chemistry. Mono-Ub labeled with the fluorescent dye NT-647 (66 nM final concentrations) was titrated with recombinant HDAC6 WT (0.3 – 9,000 nM).

Table S1. Summary of the SBVS results obtained by using Autodock Vina and GOLD molecular docking approaches to screen the Specs database against HDAC6 ZnF-UBP. 80 compounds with a Vina score lower than -8.5 kcal/mol were selected by visual inspection. Redocking experiments with GOLD allowed the selection of 40 compounds for *in vitro* studies, possessing ChemPLP scores higher than 70, and here shaded in gray.

Compound N.	SPECS ID	Score AutoDock Vina (kcal/mol)	Score ChemPLP
1	AN-989/41696299	-8.50	90.04
2	AN-465/41988292	-8.70	89.23
3	AN-789/13333006	-8.50	88.26
4	AN-329/40614390	-8.60	86.34
5	AN-465/43384096	-8.50	85.66
6	AG-227/33339007	-8.70	83.75
7	AN-652/12098442	-8.50	76.84
8	AH-487/41736332	-9.20	83.47
9	AK-778/41182453	-8.50	83.22
10	AG-690/33059012	-8.50	80.84
11	AQ-750/41790461	-8.50	78.4
12	AG-670/42465029	-8.50	77.16
13	AQ-405/33966002	-8.60	77.04
14	AE-848/34782052	-8.80	77.03
15	AL-281/15328107	-9.20	76.97
16	AN-758/41576910	-8.50	83.7
17	AG-690/37046174	-9.10	76.83
18	AG-664/42183772	-8.70	76.53
19	AG-690/40751098	-8.70	75.99
20	AN-648/14910009	-9.00	75.17
21	AK-918/15000006	-9.10	74.85
22	AH-034/32862034	-8.60	74.01
23	AG-219/11640066	-8.70	73.91
24	AJ-091/14841005	-9.00	73.67
25	AO-476/43421070	-8.50	72.81
26	AR-434/42808132	-8.60	72.68
27	AG-401/04288033	-8.50	72.48
28	AN-979/41713729	-9.00	71.44
29	AI-204/31751028	-8.70	71.97
30	AJ-292/42490180	-8.70	72.22
31	AP-853/42931451	-8.80	71.02
32	AG-690/11154068	-8.70	70.98
33	AK-693/43467054	-8.90	70.84
34	AO-854/43464344	-8.50	70.67
35	AG-670/13620005	-8.50	70.56
36	AN-698/40718570	-8.50	70.52
37	AK-918/43446497	-8.60	70.44
38	AH-628/31534016	-8.50	70.3
39	AQ-390/42869255	-8.50	70.25
40	AE-406/41056104	-8.60	70.14
41	AG-401/40683250	-8.90	69.81

42	AN-329/15517020	-8.50	69.66
43	AH-357/03534059	-8.60	69.59
44	AG-401/11255010	-8.50	69.59
45	AM-807/42860156	-8.60	69.52
46	AO-548/40099038	-8.60	68.97
47	AK-245/36478005	-8.60	68.69
48	AJ-030/12106002	-8.50	68.52
49	AE-641/00760054	-8.90	68.38
50	AH-262/37292008	-8.80	67.7
51	AL-291/37303010	-8.50	67.58
52	AO-081/41192283	-9.00	67.45
53	AN-153/14989134	-8.50	67.38
54	AG-401/36962010	-8.50	67.31
55	AK-968/40941016	-8.50	67.24
56	AO-022/43455485	-8.50	67.01
57	AH-487/11681002	-8.80	66.87
58	AO-365/12165125	-8.80	66.59
59	AN-988/14610124	-9.50	66.53
60	AF-960/00446051	-8.60	66.52
61	AO-081/15246789	-8.60	66.32
62	AP-970/41849352	-8.50	65.87
63	AP-060/41942484	-8.60	65.61
64	AK-830/13217194	-8.50	65.58
65	AQ-143/43099523	-8.50	65.58
66	AH-262/11508001	-8.50	65.19
67	AK-245/11362010	-8.50	65.17
68	AI-031/31965003	-8.70	65.06
69	AI-031/40760656	-8.60	65.05
70	AI-031/14089015	-8.70	64.86
71	AD-276/12158001	-8.50	64.61
72	AG-687/36202022	-8.80	64.58
73	AO-365/40085476	-8.60	63.64
74	AO-476/14412038	-8.50	62.68
75	AE-484/32867053	-8.80	62.58
76	AG-205/11955615	-8.50	62.55
77	AK-105/40691456	-8.50	60.96
78	AH-487/34221015	-8.60	60.68
79	AK-777/36504003	-8.60	58.97
80	AK-906/40827346	-8.70	41.84

Table S2. Effect of selected hits on HDAC6 catalytic activity.

Compound	Concentration	HDAC6 activity (%)[a]
16	100 µM	98
	50 µM	96
	25 µM	99
	5 µM	92
30	100 µM	259
	50 µM	240
	25 µM	189
	5 µM	109
TSA[b]	250 nM	7
	25 nM	43
	0.5 nM	91

[a]Mean of 2 independent experiments.
[b]Trichostatin A: positive control for the inhibition of HDAC6 activity.

Supplementary References

1. Zwick, V., Simões-Pires, C. & Cuendet, M. *J Enzyme Inhib Med Chem* **31**, 209-214 (2016).

2. Boyault, C. et al. *Embo J* **25**, 3357-66 (2006).

3. Cooper, E.M. et al. *Embo J* **28**, 621-31 (2009).

4. Dos Santos Passos, C., Simões-Pires, C.A., Carrupt, P.A., Nurisso, A. *J Biomol Struct Dyn* **34**, 2581-2598 (2016).